Nanomechanical properties of artificial lipid bilayers composed of fluid and polymerizable lipids

N. Malithi Fonseka, ¹ Fernando Teran Arce, ^{2,3,*} Hamish S. Christie, ¹ Craig A. Aspinwall, ^{1,2} and S. Scott Saavedra ^{1,2,*}

Emails: saavedra@email.arizona.edu, ftarce@email.arizona.edu

RECEIVED DATE (to be automatically inserted after your manuscript is accepted if required according to the journal that you are submitting your paper to)

¹ Department of Chemistry and Biochemistry, University of Arizona, Tucson, AZ, 85721, USA

² BIO5 Institute and Department of Biomedical Engineering, University of Arizona, Tucson, AZ, 85721, USA

³ Department of Medicine, University of Arizona, Tucson, AZ, 85721, USA

^{*} Authors to whom correspondence should be addressed.

ABSTRACT

Polymerization enhances the stability of a planar supported lipid bilayer (PSLB) but it also changes its chemical and mechanical properties, attenuates lipid diffusion, and may affect the activity of integral membrane proteins. Mixed bilayers composed of fluid lipids and poly(lipids) may provide an appropriate combination of polymeric stability coupled with the fluidity and elasticity needed to maintain the bioactivity of reconstituted receptors. Previously (Langmuir, 2019, 35, 12483-12491) we showed that binary mixtures of the polymerizable lipid bis-SorbPC and the fluid lipid DPhPC form phase-segregated PSLBs composed of nanoscale fluid and poly(lipid) domains. Here we used atomic force microscopy (AFM) to compare the nanoscale mechanical properties of these binary PSLBs with single component PSLBs. The elastic (Young's) modulus, area compressibility modulus and bending modulus of bis-SorbPC PSLBs increased upon polymerization. Before polymerization, breakthrough events at forces below 5 nN were observed but after polymerization, the AFM tip could not penetrate the PSLB up to an applied force of 20 nN. These results are attributed to the polymeric network in poly(bis-SorbPC), which increases the bilayer stiffness and resists compression and bending. In binary DPhPC/poly(bis-SorbPC) PSLBs, the DPhPC domains are less stiff, more compressible, and are less resistant to rupture and bending compared to pure DPhPC bilayers. These differences are attributed to bis-SorbPC monomers and oligomers present in DPhPC domains that disrupt the packing of DPhPC molecules. In contrast, the poly(bis-SorbPC) domains are stiffer and less compressible relative to pure PSLBs; this difference is attributed to DPhPC filling the nm-scale pores in the polymerized domains that are created during bis-SorbPC polymerization. Thus, incomplete phase segregation increases the stability of poly(bisSorbPC) but has the opposite, detrimental effect for DPhPC. Overall, these results provide guidance for design of partially polymerized bilayers for technological uses.

INTRODUCTION

Artificial lipid bilayers have many applications in biotechnology, including drug delivery, separations science, chemical sensing, and as biocompatible coatings.¹⁻⁷ Planar lipid bilayers are an artificial lipid bilayer geometry that has been widely explored for receptorbased biosensing because this type of construct provides a suitable environment for incorporating and maintaining the bioactivity of membrane-associated proteins and peptides. 4-5, 8-9 Bilayer material/mechanical properties such as elasticity, curvature, and thickness influence the structure and activity of membrane-associated proteins and peptides. 10-11 Examples include stretch-activated cation channels, G proteins, phospholipase A, and voltage-dependent ion channels. 12-15 Protein and peptide binding to lipid bilayers, partitioning of exogenous molecules, and raft formation in cell membranes also have been shown to be influenced by membrane material/mechanical properties. 10, 16 These properties depend on the structure of the constituent lipids, including the type of headgroup, the length of the tails, and functional groups on the tails. 17-22 Measuring the material/mechanical properties of lipid bilayers and correlating them with studies of the structure and activity of membrane-associated proteins and peptides should advance development of sensors and related technologies based on protein/peptide-functionalized membranes.¹⁰

Continued development of these technologies also will be advanced by enhancing membrane stability. The weak, non-covalent intermolecular interactions among the lipids in a fluid-phase bilayer may be disrupted by chemical and mechanical stresses such as exposure to solvents/surfactants, extended storage time, drying/rehydration, and vibration, leading to partial or complete loss of the bilayer structure. 1, 23-24 Consequently, considerable research has been devoted to the development of techniques to stabilize planar lipid bilayers. Polymerization of reactive lipid monomers is one approach that greatly increases bilayer stability; 1, 23-24, 28-29 however, it can alter important properties such as lateral lipid diffusion and membrane material and mechanical properties. 19, 23, 25, 30-33

Although polymerized lipid bilayers have been studied extensively for decades, to our knowledge, only three papers addressing the effect of lipid polymerization on bilayer mechanical properties have been published: a) Evans and Needham used micropipette aspiration to study several lipids;³⁴ they reported relatively low values of elastic compressibility modulus for "polymerizable lipids" for which the chemical structure was not provided. b) Binder et al.³³ reported that polymerization of diene-functionalized planar lipid multilayers resulted in a very large increase in their lateral compressibility modulus. c) El Zein et al.¹⁹ used AFM force spectroscopy to study the nanomechanical properties of supported monolayers of a bis-diacetylene lipid; they observed that polymerization resulted in ca. 14-fold and 100-fold increases in breakthrough force and Young's modulus, respectively.

Properties intermediate between those of a fully polymerized bilayer and a fluid bilayer can be obtained by mixing nonpolymerizable and polymerizable lipids. For example, we have shown that polymerization of binary mixtures of fluid-phase, nonpolymerizable lipids

and polymerizable dienoyl lipids generates planar lipid bilayers in which long-range lateral diffusion is retained as well as the activity of peptides that require fluidity to reversibly associate to form transmembrane ion channels.^{30, 35} In addition, the stability of these binary membranes is intermediate relative to the single-component bilayers.³⁵

Binary planar supported lipid bilayers (PSLBs) composed of 1,2-diphytanoyl-sn-glycero-3-phosphocholine (DPhPC), fluid-phase lipid, and 1,2-bis[10-(2',4'hexadienoloxy)decanoyl]-sn-glycero-3-phosphocholine (bis-SorbPC), a polymerizable lipid are the subject of the present study (the molecular structures are shown in Figure S1). In a previous publication, ³⁰ we showed that polymerization of DPhPC/bis-SorbPC PSLBs induces phase segregation, resulting in the formation of sub-um domains composed predominately of poly(bis-SorbPC) surrounded by a semi-continuous phase composed predominately of DPhPC;³⁰ a typical AFM image is shown in Figure 1. The poly(bis-SorbPC) domains are irregularly shaped islands, with areas of 3000-6000 nm², and the DPhPC domains are somewhat larger. The height difference between the domains, 0.3 -0.4 nm, indicates that the lipids in the upper and lower leaflets of the bilayer are mostly in registry.³⁰ The present study extends the previous publication. Here we address the questions: a) How do the mechanical properties of bis-SorbPC PSLBs change upon polymerization? b) In mixed PSLBs, do the mechanical properties of the DPhPC and poly(bis-SorbPC) domains differ from those of the pure (single-component) PSLBs?

Several techniques have been developed to study the mechanical properties of lipid bilayers, including X-ray scattering,^{36,37} Langmuir isotherms,³⁸ micropipette aspiration,^{34, 39} and AFM force spectroscopy.^{18, 21} Although micropipette aspiration has been the most widely used, it can only be applied to vesicles and it reports on macroscopic behavior averaged

over the entire vesicle; thus it cannot be used to examine the properties of individual domains in phase-segregated membranes. To examine the mechanical properties of domains in DPhPC/poly(bis-SorbPC) PSLBs, sub-µm spatial resolution is needed, which dictated the use of AFM force spectroscopy in the present study. Breakthrough force, bilayer thickness and deformation, Young's modulus, area compressibility modulus, and bending modulus were determined for pure and binary PSLBs, enabling these properties to be compared for DPhPC, bis-SorbPC, poly(bis-SorbPC) and the domains in mixed DPhPC/poly(bis-SorbPC) bilayers.

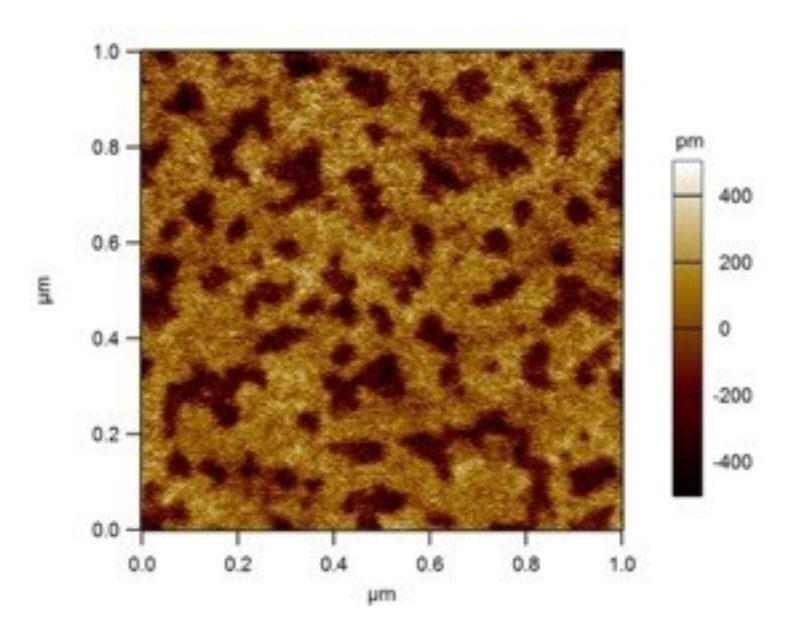


Figure 1. A tapping mode AFM image of a PSLB of composed of 1:1 (mol/mol) DPhPC and poly(bis-SorbPC). The higher regions are predominately DPhPC; the lower regions are predominately poly(bis-SorbPC). The image was obtained in phosphate buffer at room temperature. Domain sizes, heights, and other properties are described in a previous publication.³⁰

EXPERIMENTAL SECTION

Materials. DPhPC was purchased from Avanti Polar Lipids (Alabaster, AL). bis-SorbPC was synthesized in-house as previously described. 30,40 Stock solutions of bis-SorbPC were prepared in benzene. Prior to polymerization, bis-SorbPC was always handled under yellow light or in dark conditions. Water was obtained from a Barnstead Nanopure system (Thermolyne Corporation, Dubuque, IA) with a minimum resistivity of 18 MΩ·cm. Atomically smooth silicon wafers with [111] orientation were obtained from Wacker Chemie (Munich, Germany).

Preparation of PSLBs for AFM. Small unilamellar vesicles (SUVs) were prepared as previously described.³⁰ Sonication was done at 35 °C to keep bis-SorbPC above its main phase transition temperature of 28 °C.³⁰ Si wafers were cleaned in piranha solution (7:3 concentrated H₂SO₄: 30% H₂O₂) for 30 minutes, rinsed thoroughly with DI water, and dried with a stream of nitrogen. PSLBs were formed by vesicle fusion on Si wafers at 35 °C, as previously described.³⁰

To polymerize bis-SorbPC, a low-pressure mercury pen lamp (Pen-Ray Model 3SC-9, UVP, Upland, CA) with a rated intensity of 4500 μ W/cm² at 254 nm was directed through a bandpass filter (325 nm, 140 nm FWHM; U330, Edmund Optics) for 30 minutes at room temperature (24±2 °C). The distance between the lamp and the PSLB was 7.5 cm. These conditions were sufficient to photoreact >95% of the polymerizable groups in bis-SorbPC (see Supporting Information (SI); Section 2). Subsequent experiments were performed at room temperature (24±2 °C).

AFM imaging. AFM images of lipid bilayers were obtained with a Cypher S AFM (Oxford Instruments Asylum Research, Inc., Santa Barbara, CA) using Asylum Research Version 15 software running on an IGOR platform (Pro WaveMetrics, Lake Oswego, OR). All imaging was performed using TR400 PSA tips (Olympus Corporation, Center Valley, PA) in a ~100 μL liquid droplet of 10 mM phosphate buffer (pH 7.0) using contact mode, unless stated otherwise. Before use, the cantilevers were drift equilibrated and thermally stabilized in phosphate buffer for ~30 min. Images were acquired at a scan rate of 2.44 lines per second with 256 points per line. Successive scans were performed on all PSLBs and no changes in morphology were observed, showing that the films were not altered by the applied force. Images were analyzed using the Asylum Research software to remove the polynomial background.

Force mapping. Force mapping was performed under similar conditions (Cypher S AFM, 10 mM phosphate buffer, and TR400 PSA tips). The cantilever deflection sensitivity was obtained by indenting the cantilever on a clean Si wafer. The spring constants were determined by the thermal noise method,⁴¹ implemented in the equipment software. The average spring constant was 0.105 N/m (±0.006; n=6).

Prior to force mapping, an overview scan of a 1 μm² area was acquired to assess PSLB morphology, then a 200 nm x 200 nm sub-area was selected for mapping. Each map consisted of an array of 16 x 16 force curves (applied force vs. separation distance between the AFM tip and the substrate; see example in Fig. 2A). The pixel area (12.5 nm x 12.5 nm) and scan area were selected to enable analysis of the domains in 1:1 (mol/mol) DPhPC/poly(bis-SorbPC) PSLBs that have sub-μm dimensions, as shown in Figure 1 and described quantitatively in the previous publication.³⁰ The tip radius was estimated as 10

nm. For a 10 nm tip radius, the contact radius with a 5 nm thick PSLB is estimated to be 6.6 nm. The lateral resolution of force mapping is estimated to be about 5 nm and 9 nm for DPhPC and poly(bis-SorbPC) domains, respectively, in the 1:1 (mol/mol) PSLBs. These estimates are based on calculations presented in Section 4 of the SI.

A relatively low vertical tip velocity of 397 nm/s was chosen to minimize the viscosity force, which varies linearly with the tip velocity in liquid.⁴² Comparable or lower velocities have been frequently reported in the literature.^{19, 43-48} The tip was raised 200 nm above the PSLB before each force curve, consisting of 1000 data points, was measured. The time interval between successive contacts of the tip with the bilayer was approximately 1.08 s, which included 0.07 s for the tip to move laterally to an adjacent pixel. This 1.08 s time interval was sufficient for PSLBs to recover from tip indentation, as determined by measuring force curves repeatedly at a single spot and obtaining topographic images of PSLBs before and after force mapping (see Section 3 of the SI).

Force curve and force map analyses. Force curve and force map analyses were done using custom code implemented in MATLAB R2017a (MathWorks, Natick, MA, USA). Figure 2A shows labeled points and regions of a force curve corresponding to schematic representations of a tip interacting with a PSLB in Figure 2B. The breakthrough point was identified as the point in the contact region of the force curve (between point b in Fig. 2A and the maximum force applied) at which the force between two successive data points did not exceed a selected threshold (usually 0 nN). The bilayer thickness was calculated as the distance from the point at which the tip first contacted the bilayer (point b in Fig. 2A) to the position of tip-substrate contact (point d in Fig. 2A). In most force curves, tip jump-to-contact was observed at distances greater than point b (see below). The force curves that

gave unreasonable bilayer thicknesses (i.e., values <2 nm or >7 nm) were excluded from the analysis.

The Hertz model assumes a linear deformation in an infinitely thick, elastic material indented by a sphere,⁴⁹ and can be written as

$$F = \frac{4}{3}E^*\sqrt{R}h^{3/2}$$
 (1)

where F is the applied force, E^* is the reduced elastic (Young's) modulus, R is the AFM tip radius and h is the indentation depth. E^* can be calculated using,

$$\frac{1}{E^*} = \frac{\left(1 - v_{tip}^2\right)}{E_{tip}} + \frac{\left(1 - v_{PSLB}^2\right)}{E_{PSLB}} \tag{2}$$

where v_{tip} and v_{PSLB} are the Poisson's ratios of the tip and the PSLB, respectively, and E_{tip} and E_{PSLB} are the Young's moduli of the tip and the PSLB, respectively. For an AFM silicon nitride tip, $v_{tip} = 0.28$ and $E_{tip} = 165$ GPa. Lipid bilayers are considered to have limited surface compressibility or resistance to surface density changes, exhibiting solid or liquid-like behavior. Lipid bilayers are therefore considered as incompressible materials, and a Poisson's ratio (v_{PSLB}) of 0.5 is assumed. S1-52, 47

The Dimitriadis extension to the Hertz model addresses the case of a linearly-deformed elastic layer of finite thickness on a rigid substrate,⁵¹

$$F = \frac{4}{3}E^*\sqrt{R}h^{3/2}[1 + 1.133\chi + 1.283\chi^2 + 0.769\chi^3 + 0.0975\chi^4]$$
 (3)

where $\chi = \frac{\sqrt{Rh}}{d}$ and d is the bilayer thickness.

The low force, elastic region of each force curve (region c in Fig. 2A; typically 0.2 to 0.9 nN) was fit with the Dimitriadis model to obtain the elastic (Young's) modulus. 53,54,51,55 For curves with breakthrough events, we selected the upper bound of region c (i.e., the highest loading force) as 0.3 - 0.4 the value of the breakthrough force. This choice ensured that a sufficient number of data points (at least 30 and typically 40 - 50) were used in the curve fitting and, coupled with use of the Dimitriadis model, decreased the substrate contributions to the Young's modulus. 52 At higher loading forces, the force curves often deviated from elastic behavior. As shown in Figure 2A, the slight flattening of the curve above region c suggests the onset of plastic deformation. For curves without breakthrough events, we selected upper bounds of 0.9 nN for pure poly(bis-SorbPC) and 0.6 nN for poly(bis-SorbPC) domains. The quality of the fits was assessed by calculating the R^2 and visually examining the fitted curves and the residuals (see Section 5 of the SI).

From the Dimitriadis-derived Young's modulus, the area compressibility modulus (K_A) and the bending modulus (k_c) of the lipid bilayers were obtained. K_A was calculated using Equation 4, ^{52,47}

$$K_A = \frac{E_{PSLB}d}{(1 - v_{PSLB}^2)} \tag{4}$$

which is derived from thin shell theory, and k_c was calculated using Equation 5.⁴⁶

$$k_c = \frac{E_{PSLB}d^3}{24(1 - v_{PSLB}^2)} \tag{5}$$

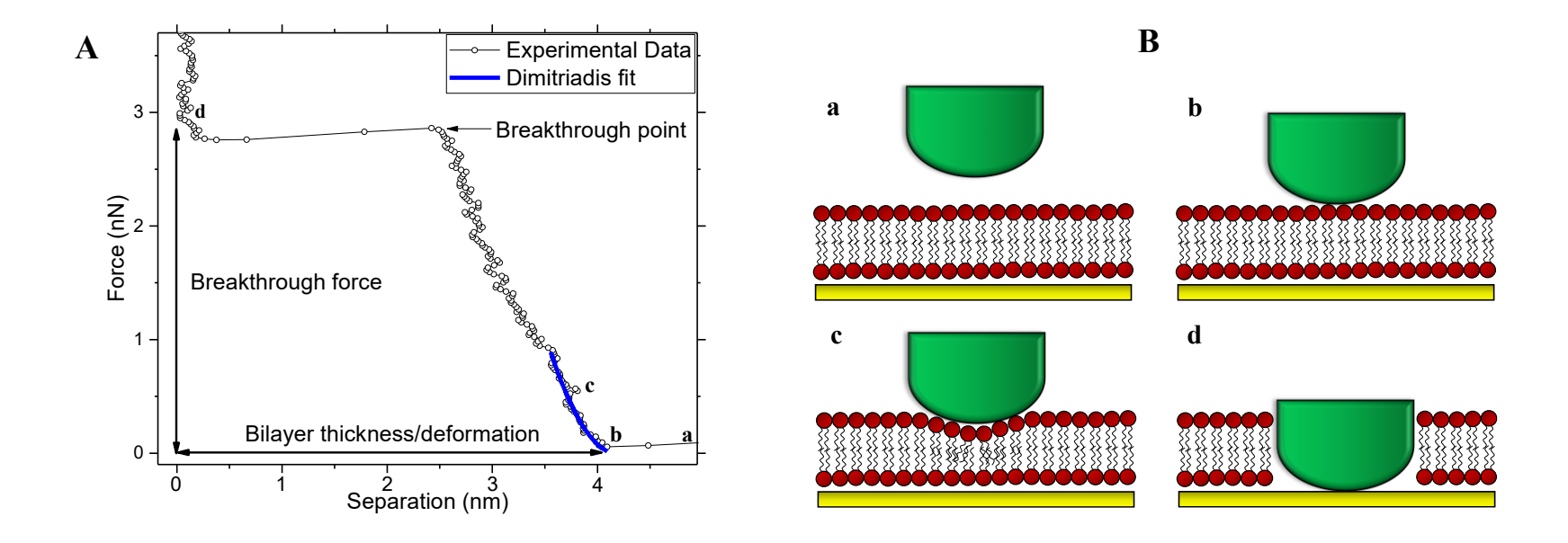


Figure 2. A. A section of a representative force curve (applied force vs. separation distance between the AFM tip and the substrate) measured on a DPhPC PSLB. The black circles are experimental data; the solid line connects the data points. B. Schematic illustrations representing tip-PSLB interactions corresponding to the different regions and points labeled on the force curve in A. In region a, the tip has not compressed the PSLB so the measured force is near zero. At point b, the tip begins to compress the PSLB. In region c, the tip experiences repulsion as the PSLB is elastically compressed. The blue line is the fit of the Dimitriadis model⁵¹ to the experimental data from which the Young's modulus is calculated. The measured force increases until the breakthrough point is reached. At the breakthrough point, the tip penetrates through the PSLB and contacts the underlying SiO₂ substrate (region d). In this region, the rate of force increase is greater because the SiO₂ substrate is not compressible. The breakthrough force is a measure of the bilayer resistance to rupture and thus its mechanical stability. From a molecular perspective, it represents the strength of the intermolecular interactions between lipids, including hydrophobic interactions between the tails and electrostatic interactions, hydrogen bonding, and water cross-bridges between the head groups.^{20,56}

For each force map, the mechanical parameters obtained from the force curves (breakthrough force, bilayer thickness or deformation, and elastic modulus) were plotted as histograms. These histograms were assumed (and appeared) to have normal statistical distributions. A Gaussian function was fit to the histogram for each parameter obtained from each force map; examples are shown in Sections 6 and 7 of the SI. The mean of the Gaussian fit from each force map was used to compute an overall mean and standard deviation from a minimum of three force maps. Adhesion forces were analyzed and adhesion force maps were generated using the Cypher S AFM software Version 15.

RESULTS AND DISCUSSION

AFM Force spectroscopy on DPhPC PSLBs. A representative force curve measured on a DPhPC PSLB, shown in Figure 3A, exhibits two apparent breakthrough events: a) a low force event at $F \approx 0.15$ nN and a tip-to-substrate separation distance $(D) \approx 6$ nm, respectively, and b) a higher force event at $F \approx 3.3$ nN and $D \approx 2.7$ nm. The lower force event is assigned to the tip jumping to contact with the upper surface of the PSLB. Jump-to-contact occurs when the van der Waals attraction between the tip and the underlying surface exceeds the longer range repulsive forces and the cantilever spring constant; ⁵⁷⁻⁵⁸ it is usually observed when an AFM force curve is measured in a low ionic strength solution, which was the case in this study ($\mu \approx 18$ mM for 10 mM phosphate buffer, pH 7). The higher force event is assigned to the tip penetrating through the PSLB and making contact with the underlying SiO₂ substrate. ^{21, 43} Both the jump-to-contact and the lipid bilayer breakthrough were routinely observed in DPhPC force curves.

The force curves were analyzed to obtain the breakthrough force, the bilayer thickness and the Young's modulus. Table 1 summarizes the breakthrough force obtained from 25 force maps collected from five individually prepared DPhPC PSLBs and using different AFM tips. The standard deviation was ± 1 nN, which was sufficiently small to distinguish between the different types of PSLBs studied here (see below). It also shows that making measurements on multiple samples and using several different AFM tips did not introduce a large degree of uncertainty (see Section 7 in SI for a list of DPhPC samples and AFM tips from which ± 1 nN was calculated; also presented are example histograms from individual force maps measured on different areas of different samples using different tips).

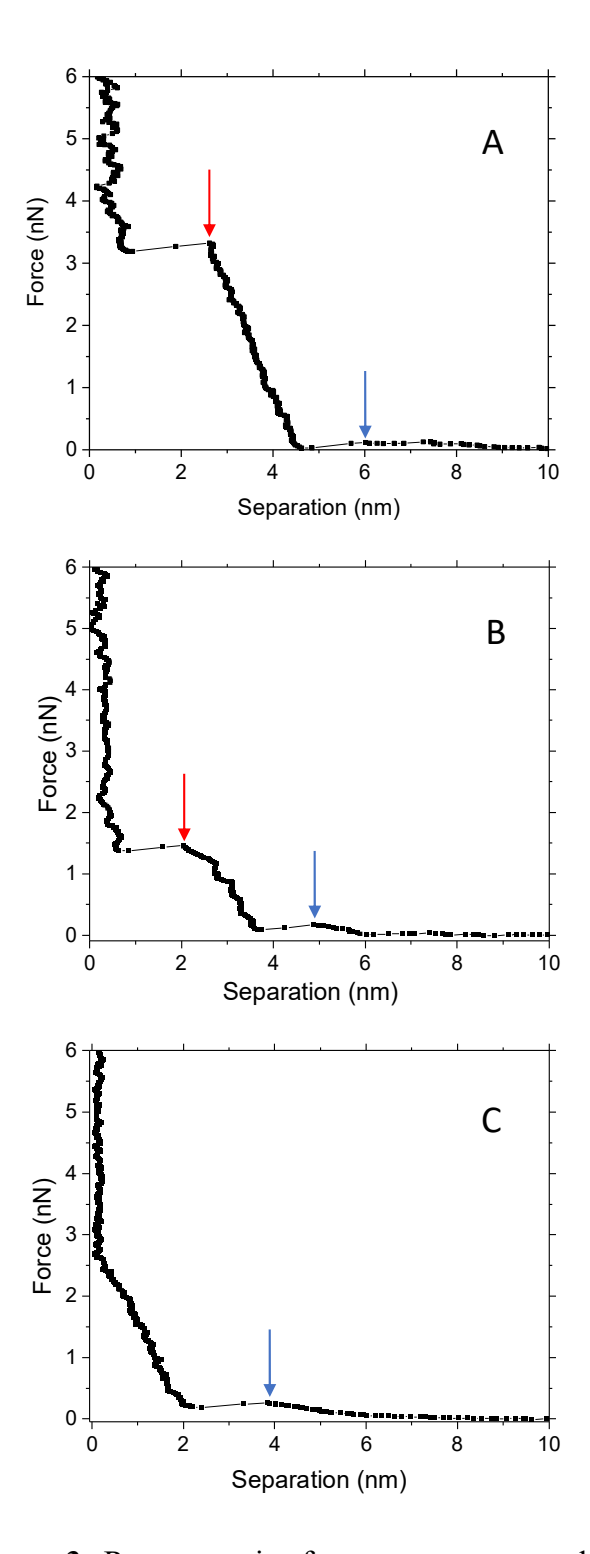


Figure 3. Representative force curves measured on pure PSLBs composed of DPhPC (**A**), bis-SorbPC (**C**), and poly(bis-SorbPC) (**E**). The blue arrows mark the tip jump-to-contact in each curve. The red arrows mark the lipid bilayer breakthrough, if present, in each curve.

Table 1. Breakthrough force and the bilayer thickness measured for DPhPC and bis-SorbPC PSLBs.

Parameter	DPhPC	bis-SorbPC b
Breakthrough force (nN) ^c	3.5 ± 1 ^a	1.5 ± 0.4
Bilayer thickness (nm) ^c	4.9 ± 1 ^b	3.8 ± 0.3

^a Data obtained from five individually prepared samples, with more than 700 force curves on each sample, and using six independently calibrated AFM tips. ^b Data obtained from three or more individually prepared samples, with more than 700 force curves on each sample, and three or more independently calibrated AFM tips. ^c Errors are ±1 standard deviation.

The mean breakthrough force for DPhPC PSLBs, 3.5 nN (Table 1), is comparable to breakthrough forces reported in the literature for various types of fluid PSLBs (0.5 - 4 nN), ^{59,47,60,61,45,44,62,63} but lower than breakthrough forces previously reported for DPhPC (8 – 12 nN). ^{20,64} The difference between the DPhPC literature values and the value reported here is attributed to the comparatively low ionic strength of 10 mM phosphate buffer and the low velocity of the AFM tip approaching the surface. Cations promote more compact bilayer structures, and thus higher ionic strength buffers increase the breakthrough force of PSLBs. ⁵⁶ Furthermore, the AFM tip velocity used here (397 nm/s) was lower than the velocity used in the previous studies (1000 nm/s). ^{64,20} A higher tip velocity is known to increase the breakthrough force, because at higher force loading rates, the time interval in which the rupture event can occur is shorter than at lower force loading rates. ^{49,60,44,56}

The bilayer thickness obtained for DPhPC was 4.9 nm (Table 1). This value is slightly higher than the thickness of 4.0 nm obtained in our previous study³⁰ by topographical

imaging of scratches made with an AFM tip, however, the agreement is reasonable given the significant differences in how the measurements were made.

The Young's modulus of DPhPC determined using the Dimitriadis model was 50 MPa (Table 2) which, to our knowledge, is the first reported Young's modulus for DPhPC. Our value is within the range of published Young's moduli, 5 – 64 MPa, measured by AFM on fluid phase bilayers composed of PC lipids. 17, 46-48, 52, 65-66 In these studies, several different models were used to calculate the Young's modulus which is a likely contributor to the spread in the values. Other contributing factors are discussed below.

Table 2. Moduli of DPhPC, bis-SorbPC, and poly(bis-SorbPC) PSLBs.

Parameter	DPhPC	bis-SorbPC	poly(bis- SorbPC)
Young's modulus from Dimitriadis model (MPa) ^{a,b}	50±40	20±9	60±20
K_A estimated from Dimitriadis model (N/m) ^c	0.33	0.13	0.39
k_c estimated from Dimitriadis model (J) ^d	3.3×10^{-19}	0.78×10^{-19}	1.6×10^{-19}

^a Data obtained from three or more individually prepared samples with more than 700 force curves on each sample, and using three or more independently calibrated AFM tips. Errors are \pm one standard deviation. ^b Calculated using Equation 3. ^c Calculated using Equation 4. ^d Calculated using Equation 5.

The calculated value for the area compressibility modulus (K_A) is 0.33 N/m (Table 2). This value is about 3-fold higher than the lateral compressibility modulus of 0.122 N/m obtained from the pressure-area isotherm of a DPhPC monolayer spread at the air-water interface (at the monolayer-bilayer equivalence pressure for DPhPC, which is 40 mN/m).⁶⁷ K_A values

for other types of fluid phase, PC lipid bilayers have been published: a) 0.22 - 0.26 N/m was measured for 12 different lipids using micropipette aspiration on giant vesicles;³⁹ and b) AFM force spectroscopy on supported DOPC bilayers yielded $K_A \approx 0.11$ N/m.^{46-47, 68}

The estimated bending modulus (k_c) obtained using the Dimitriadis model is 3.3 x 10⁻¹⁹ J (Table 2). This value is a factor of 2-6 greater than than published data: a) k_c values of 0.52 x 10⁻¹⁹ J and 0.74 x 10⁻¹⁹ J were measured by X-ray scattering on unilamellar DPhPC and DOPC vesicles, respectively;³⁷ b) a more recent X-ray scattering of multilamellar lipid films yielded $k_c = 0.61 \text{ x } 10^{-19} \text{ J}$ for DPhPC and 0.67 x 10⁻¹⁹ J for DOPC;³⁶ c) Table 2 in Et-Thakafy, et al.¹⁷ lists k_c values for DOPC PSLBs and liposomes, obtained using AFM methods, in the range of 0.88 - 1.69 x 10⁻¹⁹ J; d) $k_c = 1.56 \text{ x } 10^{-19} \text{ J}$ was measured for DOPC PSLBs, also using AFM;⁴⁶ and e) k_c values of 0.38 - 1.2 x 10⁻¹⁹ J were measured for 12 different lipids using micropipette aspiration on giant vesicles.³⁹

Our value for the Young's modulus of DPhPC, 50 MPa, is near the upper bound of the range of published moduli, 5-64 MPa. Given that K_A and k_c are calculated from E_{PSLB} in equations 4 and 5, our estimated values for these moduli are also expected to be high relative to the range of the published values. This in part explains the differences between our K_A and k_c estimates and the published data cited above. The inherent uncertainties in AFM force spectroscopy are probably a more important contributor. As discussed elsewhere, $^{51, 66, 69}$ numerous factors can influence the accuracy of moduli obtained from force spectroscopy measurements, including inaccuracies in determining the deflection sensitivity, the spring constant, and the tip geometry, uncertainties in identifying the tip-sample contact point and the regions of elastic vs. plastic deformation, and the use of different theoretical models that vary in their underlying assumptions. Despite these

uncertainties, we point out that within this study, moduli for different lipids and bilayer compositions can be quantitatively compared; e.g., the moduli of DPhPC and poly(bis-SorbPC) in pure and binary PSLBs.

AFM force spectroscopy on bis-SorbPC and poly(bis-SorbPC) PSLBs. Force spectroscopy studies on bis-SorbPC PSLBs were performed at room temperature which is below the T_m of 28 °C.³⁰ Similar to DPhPC, both a jump-to-contact and a lipid bilayer breakthrough were routinely observed in bis-SorbPC force curves. A representative force curve, shown in Figure 3B, exhibits the jump-to-contact at $F \approx 0.17$ nN and $D \approx 5.1$ nm and the bilayer breakthrough at $F \approx 1.5$ nN and $D \approx 2.2$ nm.

Quantitative analysis of bis-SorbPC force maps yielded an average PSLB thickness of 3.8 nm (Table 1), about 1 nm less than that of DPhPC. This value is somewhat lower than the thickness of 4.4 nm obtained in a previous study³⁰ by topographical imaging of scratches in a bis-SorbPC PSLB with an AFM tip but, as noted above, the agreement is reasonable given the significant differences in how the measurements were made.

The average breakthrough force of bis-SorbPC PSLBs was 1.5 nN (Table 1), which is less than half of the value observed for DPhPC PSLBs. DPhPC contains saturated 16-carbon tails with four methyl braches per tail, whereas the tails in bis-SorbPC contain sorbyl esters and are longer than the DPhPC tails by about the length of a C-O bond (see structures in Section 1 of the SI). Force spectroscopy studies of PC lipids have shown that increasing the chain length causes an increase in the breakthrough force, whereas chain branching has the opposite effect due to the branches causing distortions in molecular packing.²⁰ Although these factors suggest that a DPhPC PSLB should have a lower breakthrough force than a bis-SorbPC PSLB, our results suggest that the sorbyl esters have a stronger influence.

The same study²⁰ showed that introducing a *cis* unsaturation in one tail of the lipid decreased the breakthrough force due to the inherent packing distortions. The two *trans* double bonds and the ester group in the bis-SorbPC tails should also cause significant packing disruptions relative to saturated tails, with a consequently lower breakthrough force. Another study from our laboratory showed that suspended bis-SorbPC bilayers are significantly more porous to K⁺ than suspended DPhPC bilayers,²³ which also suggests that the tails in bis-SorbPC PSLBs are packed less densely and less organized relative to the tails in DPhPC PSLBs.

The Young's modulus of bis-SorbPC determined using the Dimitriadis model was 20 MPa from which $K_A = 0.13$ N/m and $k_c = 7.8 \times 10^{-20}$ J were calculated (Table 2). These data show that bis-SorbPC bilayers are less stiff, more compressible, and have a lower resistance to bending compared to DPhPC bilayers.

The nanomechanical properties of bis-SorbPC PSLBs that were polymerized via UV irradiation were found to be significantly different from those of unpolymerized bis-SorbPC PSLBs. An example force curve is shown in Figure 3C. The tip jump-to-contact occurs at $F \approx 0.25$ nN and $D \approx 3.8$ nm and, similar to DPhPC and bis-SorbPC, was routinely observed in poly(bis-SorbPC) force curves (see histogram in Figure S12). However, in contrast to the DPhPC and bis-SorbPC results, lipid bilayer breakthrough is not present in Figure 3C. (Note: The $D \approx 3.8$ nm for the jump-to-contact is apparent because the tip did not make contact with the substrate). In 85% of the poly(bis-SorbPC) force curves that were analyzed, no bilayer breakthrough events were observed with applied forces up to 20 nN. The absence of bilayer breakthrough shows that poly(bis-SorbPC) is much more resistant to rupture compared to unpolymerized bis-SorbPC, which is attributed to the

presence of the polymeric network near the center of the bilayer. Figure 4 shows a schematic illustration of an AFM tip deforming but not penetrating a poly(bis-SorbPC) bilayer. These results complement our previous studies which reported enhanced stability of poly(bis-SorbPC) PSLBs, e.g., their resistance to desorption when treated with surfactants,²⁴ however this is the first study to examine the nanomechanical stability of poly(bis-SorbPC).

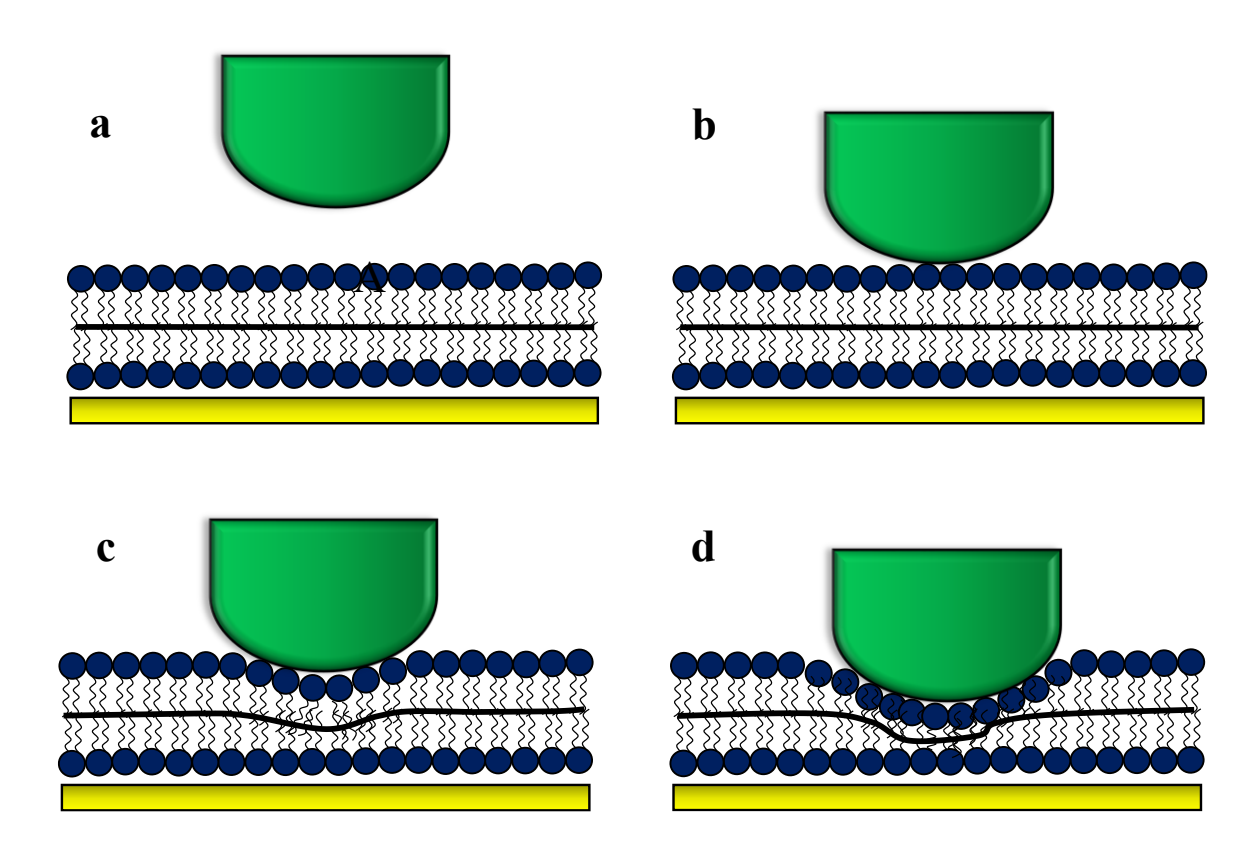


Figure 4. Schematic illustration of a poly(bis-SorbPC) PSLB during deformation by an AFM tip. The black line in the center of the bilayer indicates the region where the polymeric network is located. **a.** Before the tip contacts the PSLB contact. **b.** At contact. **c** and **d.** The tip compresses the PSLB but even with application of a relatively high force (~20 nN), breakthrough does not occur.

The absence of AFM tip penetration into a supported lipid bilayer at relatively high force has been observed previously. Zou and coworkers studied bilayers composed of DOPC, sphingomyelin, cholesterol, and ceramide.^{22, 70} Ceramide-enriched domains were inpenetrable at loading forces up to 70 nN, which was ascribed to very tight molecular packing promoted by strong intermolecular interactions.

Due to the absence of a breakthrough event, the bilayer thickness of poly(bis-SorbPC) could not be determined from force curves. The average deformation of poly(bis-SorbPC) under a force of 10 nN was 2.2 (±0.1) nm. In our previous study, tapping mode AFM was used to obtain an apparent thickness of 3.6 (±0.3) nm for poly(bis-SorbPC) PSLBs.³⁰ The ratio of these numbers indicates that at 10 nN, the bilayer deformation relative to its initial thickness (i.e., the strain) is about 60%. In comparison, DPhPC deforms about 30% before rupture occurs; in the case of bis-SorbPC, it is about about 40%. Therefore, poly(bis-SorbPC) can resist greater strains and stresses without rupturing (i.e., it has more ductile character as compared to DPhPC and bis-SorbPC).

Upon polymerization, the Young's modulus of poly(bis-SorbPC) increased from 20 MPa to 60 MPa (Table 2) which is indicative of a stiffer bilayer. A much larger increase was reported by El Zein, et al.¹⁹ for supported monolayers of 1,2-bis(10,12-tricosadiynoyl)-*sn*-glycero-3-phosphocholine (DC8,9PC); upon polymerization, the Young's modulus (determined using the Hertz model) increased from 2.0 MPa to 229 MPa.¹⁹ A larger increase compared to bis-SorbPC is not surprising as bis-diacetylenic lipid polymerization generates a highly cross-linked polymer in which lateral diffusion is eliminated on the timescale of a FRAP measurement.^{32,71} In addition, polymerization of bis-SorbPC creates

a porous bilayer^{23,72} which likely produces a more compressible material relative to poly(DC8,9PC) (see discussion below).

Since the poly(bis-SorbPC) thickness could not be determined from the force-distance curves, an estimated bis-SorbPC thickness, corrected for shrinkage during polymerization, was used to calculate K_A and k_c for poly(bis-SorbPC). Specifically, the ratio of the thicknesses of poly(bis-SorbPC) to bis-SorbPC that were measured by AFM imaging of scratches made in PSLBs was $0.82.^{30}$ Applying this ratio to the bis-SorbPC thickness measured here (Table 1) yields an estimated poly(bis-SorbPC) thickness of 3.1 nm. Using this value for d, $K_A = 0.39$ N/m and $k_c = 1.6$ x 10^{-19} were calculated for poly(bis-SorbPC). These moduli are greater than the K_A and k_c of unpolymerized bis-SorbPC, showing that polymerization produces a stiffer bilayer.

Force spectroscopy studies on bilayers composed of equimolar DPhPC and poly(bis-SorbPC). PSLBs composed of DPhPC and bis-SorbPC undergo polymerization-induced phase segregation, forming DPhPC and poly(bis-SorbPC) domains.³⁰ In the example AFM image shown in Figure 1, the taller, semi-continuous DPhPC phase surrounds the shorter islands of poly(bis-SorbPC). Here the nanomechanical properties of mixed PSLBs composed of DPhPC and poly(bis-SorbPC) (1:1 mol/mol) were examined.

An example set of data is shown in Figure 5. A comparison of the AFM height image (Fig. 5A) and the corresponding breakthrough force map (Fig. 5B) shows that regions in which breakthrough events were observed coincide with the taller DPhPC domains in the height image. The regions in the force map in which breakthrough events were not observed coincide with the lower poly(bis-SorbPC) domains in the height image. In the corresponding thickness/deformation map (Fig. 5C), the high and low regions coincide

with the DPhPC and poly(bis-SorbPC) domains, respectively, in the height image. These observations are consistent with the results obtained from pure PSLBs of DPhPC and poly(bis-SorbPC). The Young's modulus (Fig. 5D) map also correlates well with the height image.

In the analysis of these maps, the criteria used to identify poly(bis-SorbPC) regions were defined as the lack of a breakthrough event and a deformation ≤ 2.2 nm. For the DPhPC domains, the criteria were observation of a breakthrough event and a bilayer thickness greater than 2.2 nm. Example force curves for poly(bis-SorbPC) and DPhPC domains are shown in Figure 6; both show a tip jump-to-contact whereas a lipid bilayer breakthrough is observed only for DPhPC, consistent with results for pure PSLBs.

The breakthrough force observed for DPhPC domains in mixed bilayers is 0.9 nN (Table 3), which is four-fold lower than the breakthrough force measured for pure DPhPC PSLBs (Table 1). Similarly: a) The thickness of the DPhPC domains, 3.1 nm (Table 3), is lower than the value of 4.9 nm (Table 1) observed for pure DPhPC bilayers. b) The Young's modulus of the DPhPC domains, 30 MPa, is lower than the 50 MPa (Table 2) obtained for pure DPhPC bilayers. c) The K_A and k_c values for the DPhPC domains are lower than the corresponding values for pure DPhPC bilayers listed in Table 2.

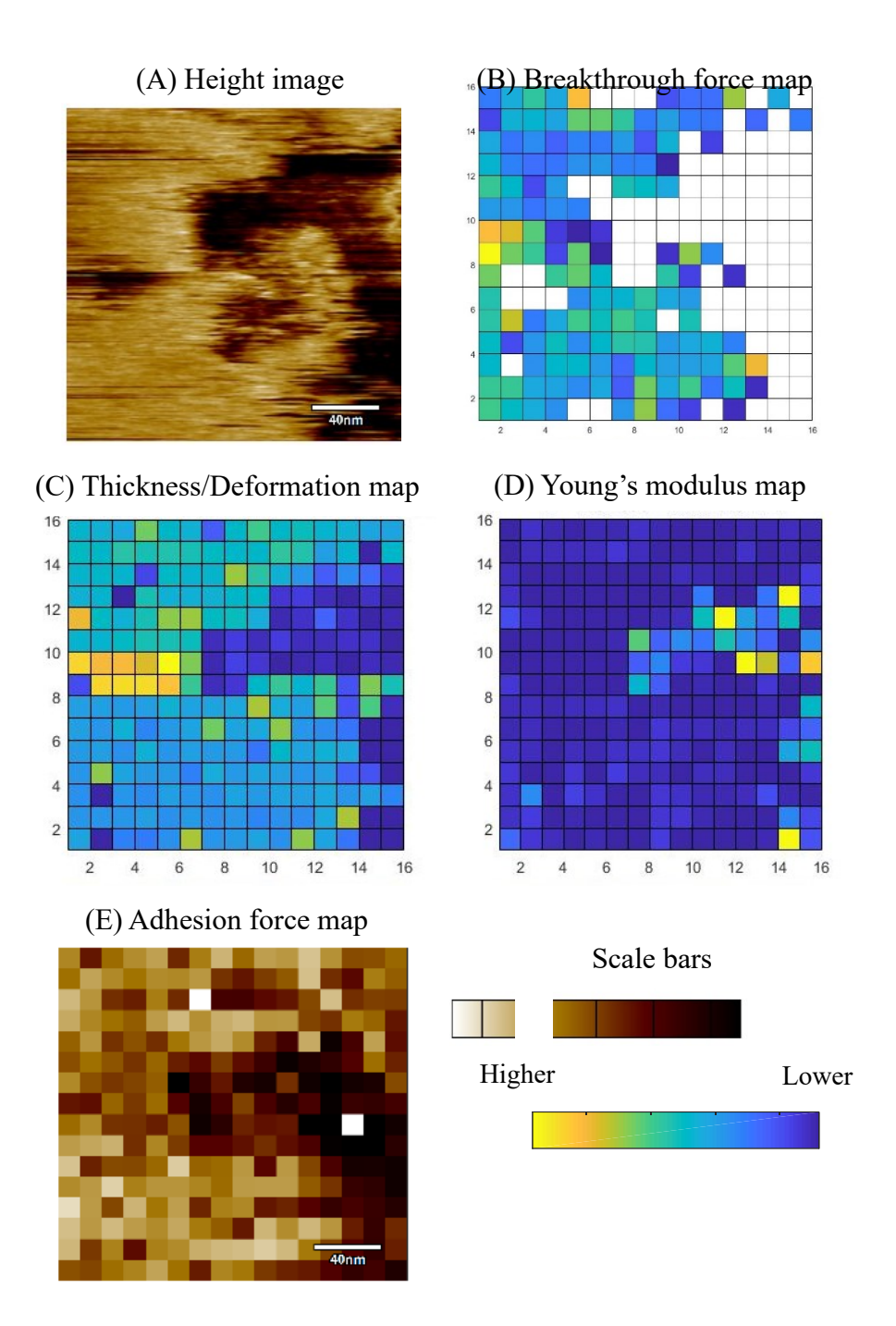


Figure 5. Force spectroscopy on a 200 nm X 200 nm area of a mixed PSLB composed of equimolar DPhPC/poly(bis-SorbPC). (A) A height image of a 200 nm x 200 nm area of the PSLB containing both DPhPC and poly(bis-SorbPC) domains (the height scale is -2.50 -2.50 nm). (B) The breakthrough force map of the region shown in (A) (the force scale is 0 - 1.5 nN). White squares represent force curves where no breakthrough events were observed. (C) The bilayer thickness/deformation map (the scale is 0 - 6 nm). (D) The Young's modulus map (the scale is 0 - 200 MPa). (E) The adhesion force map (the scale is 0.41 - 1.36 nN). White squares represent force curves that were eliminated from the analysis.

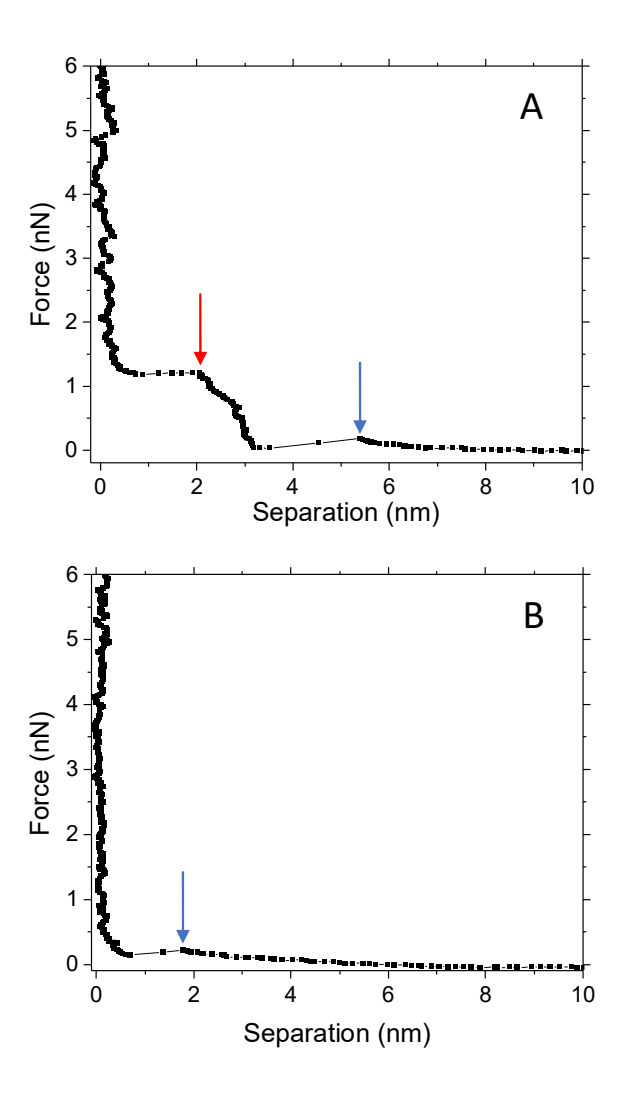


Figure 6. Representative force-distance curves measured on a DPhPC domain (**A**) and a poly(bis-SorbPC) domain (**B**) in a mixed PSLB. The blue arrows mark the tip jump-to-contact in each curve. The red arrow marks the lipid bilayer breakthrough in DPhPC.

Table 3. Summary of the breakthrough force, bilayer thickness, bilayer deformation, Young's moduli, K_A and k_c of DPhPC domains and poly(bis-SorbPC) domains in equimolar PSLBs.

Parameter	DPhPC	Poly(bis-SorbPC)
Breakthrough force (nN) ^a	0.9±0.3 ^e	-
Bilayer thickness/deformation (nm) ^a	3.1±0.3	0.7±0.1
Young's modulus from Dimitriadis model (MPa) a,b	30±10	170±30
<i>K</i> _A estimated from Dimitriadis model (N/m) ^c	0.12	0.70
k_c estimated from Dimitriadis model (J) ^d	0.50×10^{-19}	2.8×10^{-19}

^a Data obtained from three individually prepared samples, with a minimum of 256 force curves measured on each sample, and using three independently calibrated AFM tips. Errors are ± one standard deviation. ^b Calculated using Equation 3. ^b Calculated using Equation 4. ^d Calculated using Equation 5. ^e Pooled standard deviation calculated from the standard deviations of the Gaussian fits to the histrograms obtained from three force maps.

Overall, comparing the DPhPC data in Tables 1, 2, and 3 shows that the DPhPC domains in mixed PSLBs are thinner, less stiff, more compressible, and offer a lower resistance to rupture and bending compared to pure DPhPC bilayers. These differences are likely due to impurities, specifically bis-SorbPC monomers and oligomers, present in DPhPC domains, which should disrupt the packing of DPhPC molecules. A contributing factor may be differences in the properties of DPhPC domains at their edges relative to the center. It has been shown that the lateral interactions of lipids are weaker at the edges of bilayer islands, leading to a 1.3 to 2.8-fold regional difference in the breakthrough force, as well as a greater degree of freedom for lipids, i.e., the packing density is lower at the edges compared to the center. Similarly, the less ordered environment at DPhPC/poly(bis-

SorbPC) domain boundaries may contribute to the lower breakthrough force of DPhPC in mixed PSLBs.

The properties of poly(bis-SorbPC) domains in mixed PSLBs, listed in Table 3, differed from the properties of pure poly(bis-SorbPC) bilayers listed in Table 2, but the trends were mostly opposite to those observed for DPhPC: a) The Young's modulus increased to 170 MPa from 60 MPa in pure PSLBs. b) K_A and k_c values also were higher than the corresponding values for pure poly(bis-SorbPC) bilayers listed in Table 2. c) The deformation was 0.7 nm under a force of 10 nN, less than the 2.2 nm measured for pure PSLBs.

Overall, comparing the poly(bis-SorbPC) data in Tables 2 and 3 shows that the poly(bis-SorbPC) domains in mixed PSLBs are stiffer and less compressible compared to pure poly(bis-SorbPC) bilayers. We hypothesize that these differences are due to a "filling effect" provided by DPhPC. UV-initiated polymerization of a bis-SorbPC bilayer causes it to shrink and form small pores.^{23,72} Previous work showed that the maximum pore diameter formed in poly(bis-SorbPC) liposomes is 2.6 nm, and that binary vesicles composed of DOPC and poly(bis-SorbPC) contained fewer pores as the DOPC mole fraction increased, suggesting that the pores are occupied by DOPC molecules.⁷² In binary DPhPC/poly(bis-SorbPC) PSLBs, these pores are likely filled by DPhPC molecules. This increase in packing density would make the domain less compressible relative to pure poly(bis-SorbPC), leading to the differences in properties described above.

The adhesion force map that corresponds to the AFM height image, shown in Figure 5E, also correlates well with the domain locations in the height image. Due to the breakthrough that occurs in the DPhPC domains, the contact area of the AFM tip with DPhPC is larger

than for poly(bis-SorbPC) for which breakthrough does not occur. This higher tip-lipid contact area produces a higher adhesion force for DPhPC domains compared to poly(bis-SorbPC) domains.

CONCLUSIONS

The nanomechanical properties of pure (single component) DPhPC and bis-SorbPC PSLBs were compared. Bis-SorbPC bilayers have a lower resistance to rupture, a lower Young's modulus, and a lower resistance to bending compared to DPhPC bilayers. This suggests that the sorbyl moieties disrupt the packing of bis-SorbPC lipids, reducing their intermolecular interactions relative to the saturated, branched tails of DPhPC.

The resistance to rupture, the Young's modulus, and the bending modulus of bis-SorbPC increased upon polymerization, showing that polymerization generated a stiffer bilayer. The absence of a breakthrough event was the most prominent difference between unpolymerized and polymerized bis-SorbPC; this absence is attributed to the polymeric network which prevents the AFM tip from fully penetrating the PSLB.

The nanomechanical properties of binary PSLBs of DPhPC and poly(bis-SorbPC) were compared to those of the single component PSLBs. The DPhPC domains in mixed PSLBs are thinner, less stiff, more compressible, and offer a lower resistance to rupture and bending compared to pure DPhPC bilayers. These differences are attributed due to bis-SorbPC monomers and oligomers present in DPhPC domains that disrupt the packing of DPhPC molecules. In contrast, poly(bis-SorbPC) domains were stiffer and less compressible in mixed PSLBs relative to pure PSLBs; this difference is attributed to

DPhPC filling the nm-scale pores in the bis-SorbPC domains that are created during polymerization. Incomplete phase segregation therefore increased the stability of poly(bis-SorbPC) but had the opposite effect on DPhPC, decreasing its stability.

Overall, this work extends our knowledge of the properties of PSLBs composed of fluid and polymerized lipids. These materials may be suitable platforms for protein-based biosensors, where the DPhPC domains provide a fluid environment for protein reconstitution and the polymerized domains provide for bilayer stability. However, the presence of bis-SorbPC monomers and oligomers in DPhPC domains may be problematic with respect to bilayer stability and biocompatibility. In a more optimal bilayer composition, the oligomers and unreacted monomers would be excluded from the fluid lipid domains while simultaneously the fluid lipids would fill the pores in the poly(lipid) domains.

SUPPORTING INFORMATION AVAILABLE

Lipid structures, UV polymerization time, AFM images of DPhPC PSLBs before and after force mapping, force curves measured repeatedly at one spot on a DPhPC PSLB, SEM of AFM tips, lateral resolution and contact diameter estimates, error analysis for Dimitriadis fits, histograms of parameters obtained from force maps, variability in force mapping results due to the use of different AFM tips on different samples, histogram of tip jump-to-contact events. This material is available free of charge via the Internet at http://pubs.acs.org.

ACKNOWLEDGMENTS

Research reported in this publication was partially supported by the National Institute of Biomedical Imaging and Bioengineering under Award Number R01EB007047 and partially supported by the National Science Foundation under Grant No. 2003297. The content is solely the responsibility of the authors and does not necessarily represent the official views of the National Institutes of Health. Any opinions, findings, and conclusions or recommendations expressed in this material are those of the authors and do not necessarily reflect the views of the National Science Foundation. Partial support of this research also was provided by the Department of Medicine, University of Arizona. All Cypher AFM images and data were collected in the W.M. Keck Center for Nano-Scale Imaging in the Department of Chemistry and Biochemistry at the University of Arizona. Acquisition of this instrument was supported by the National Science Foundation under Grant Number 1337371.

REFERENCES

- 1. Zhang, H.; Joubert, J. R.; Saavedra, S. S., Membranes from Polymerizable Lipids. In *Polymer Membranes/Biomembranes*, Meier, W. P.; Knoll, W., Eds. Springer-Verlag Berlin: Berlin, 2010; Vol. 224, pp 1-42.
- 2. Liu, Q.; Boyd, B. J., Liposomes in Biosensors. *Analyst* **2013**, *138*, 391-409.
- 3. Sriraman, S. K.; Torchilin, V. P., Recent Advances with Liposomes as Drug Carriers. In *Advanced Biomaterials and Biodevices*, Scrivener Publishing LLC: 2014; pp 79–120.
- 4. Castellana, E. T.; Cremer, P. S., Solid Supported Lipid Bilayers: From Biophysical Studies to Sensor Design. *Surf. Sci. Rep.* **2006**, *61*, 429-444.
- 5. Reimhult, E.; Kumar, K., Membrane Biosensor Platforms Using Nano- and Microporous Supports. *Trends Biotechnol.* **2008**, *26*, 82-9.

- 6. Mansfield, E.; Ross, E. E.; Aspinwall, C. A., Preparation and Characterization of Cross-Linked Phospholipid Bilayer Capillary Coatings for Protein Separations. *Analytical Chemistry* **2007**, *79*, 3135-3141.
- 7. Morigaki, K.; Tanimoto, Y., Evolution and Development of Model Membranes for Physicochemical and Functional Studies of the Membrane Lateral Heterogeneity. *Biochimica Et Biophysica Acta-Biomembranes* **2018**, *1860*, 2012-2017.
- 8. Zhong, L.; Tu, R.; Gilchrist, M. L., Tether-Supported Biomembranes with Alpha-Helical Peptide-Based Anchoring Constructs. *Langmuir* **2013**, *29*, 299-307.
- 9. Chadli, M.; Rebaud, S.; Maniti, O.; Tillier, B.; Cortes, S.; Girard-Egrot, A., New Tethered Phospholipid Bilayers Integrating Functional G-Protein-Coupled Receptor Membrane Proteins. *Langmuir* **2017**, *33*, 10385-10401.
- 10. Andersen, O. S.; Koeppe, R. E., II, Bilayer Thickness and Membrane Protein Function: An Energetic Perspective. *Annu. Rev. Biophys. Biomol. Struct.* **2007**, *36*, 107-30.
- 11. Phillips, R.; Ursell, T.; Wiggins, P.; Sens, P., Emerging Roles for Lipids in Shaping Membrane-Protein Function. *Nature* **2009**, *459*, 379-385.
- 12. Suchyna, T. M.; Tape, S. E.; Koeppe, R. E.; Andersen, O. S.; Sachs, F.; Gottlieb, P. A., Bilayer-Dependent Inhibition of Mechanosensitive Channels by Neuroactive Peptide Enantiomers. *Nature* **2004**, *430*, 235-240.
- 13. Subramaniam, V.; D'Ambruoso, G. D.; Hall, H. K.; Wysocki, R. J.; Brown, M. F.; Saavedra, S. S., Reconstitution of Rhodopsin into Polymerizable Planar Supported Lipid Bilayers: Influence of Dienoyl Monomer Structure on Photoactivation. *Langmuir* **2008**, *24*, 11067-11075.
- 14. Brown, M. F., Curvature Forces in Membrane Lipid-Protein Interactions. *Biochemistry* **2012**, *51*, 9782-9795.
- 15. Subramaniam, V.; Alves, I. D.; Salgado, G. F. J.; Lau, P.-W.; Wysocki, R. J.; Salamon, Z.; Tollin, G.; Hruby, V. J.; Brown, M. F.; Saavedra, S. S., Rhodopsin Reconstituted into a Planar-Supported Lipid Bilayer Retains Photoactivity after Cross-Linking Polymerization of Lipid Monomers. *J. Am. Chem. Soc.* **2005**, *127*, 5320-5321.
- 16. McIntosh, T. J.; Simon, S. A., Roles of Bilayer Material Properties in Function and Distribution of Membrane Proteins. *Annu. Rev. Biophys. Biomol. Struct.* **2006**, *35*, 177-198.
- 17. Et-Thakafy, O.; Delorme, N.; Gaillard, C.; Meriadec, C.; Artzner, F.; Lopez, C.; Guyomarc'h, F., Mechanical Properties of Membranes Composed of Gel-Phase or Fluid-Phase Phospholipids Probed on Liposomes by Atomic Force Spectroscopy. *Langmuir* **2017**, *33*, 5117-5126.

- 18. Das, C.; Sheikh, K. H.; Olmsted, P. D.; Connell, S. D., Nanoscale Mechanical Probing of Supported Lipid Bilayers with Atomic Force Microscopy. *Phys. Rev. E, Stat. Nonlin. Soft Matter Phys.* **2010**, *82*, 041920.
- 19. El Zein, R.; Dallaporta, H.; Charrier, A. M., Supported Lipid Monolayer with Improved Nanomechanical Stability: Effect of Polymerization. *J. Phys. Chem. B* **2012**, *116*, 7190-5.
- 20. Garcia-Manyes, S.; Redondo-Morata, L.; Oncins, G.; Sanz, F., Nanomechanics of Lipid Bilayers: Heads or Tails? *J. Am. Chem. Soc.* **2010**, *132*, 12874-12886.
- 21. Garcia-Manyes, S.; Sanz, F., Nanomechanics of Lipid Bilayers by Force Spectroscopy with AFM: A Perspective. *Biochimica et Biophysica Acta Biomembranes* **2010**, *1798*, 741-749.
- 22. Sullan, R. M.; Li, J. K.; Zou, S., Direct Correlation of Structures and Nanomechanical Properties of Multicomponent Lipid Bilayers. *Langmuir* **2009**, *25*, 7471-7.
- 23. Heitz, B. A.; Xu, J.; Jones, I. W.; Keogh, J. P.; Comi, T. J.; Hall, H. K., Jr.; Aspinwall, C. A.; Saavedra, S. S., Polymerized Planar Suspended Lipid Bilayers for Single Ion Channel Recordings: Comparison of Several Dienoyl Lipids. *Langmuir* **2011**, *27*, 1882-90.
- 24. Ross, E. E.; Rozanski, L. J.; Spratt, T.; Liu, S. C.; O'Brien, D. F.; Saavedra, S. S., Planar Supported Lipid Bilayer Polymers Formed by Vesicle Fusion. 1. Influence of Diene Monomer Structure and Polymerization Method on Film Properties. *Langmuir* **2003**, *19*, 1752-1765.
- 25. Sisson, T. M.; Lamparski, H. G.; Kolchens, S.; Elayadi, A.; O'Brien, D. F., Cross-Linking Polymerizations in Two-Dimensional Assemblies. *Macromolecules* **1996**, *29*, 8321-8329.
- 26. Holden, M. A.; Jung, S. Y.; Yang, T.; Castellana, E. T.; Cremer, P. S., Creating Fluid and Air-Stable Solid Supported Lipid Bilayers. *J. Am. Chem. Soc.* **2004**, *126*, 6512-3.
- 27. Daniel, S.; Albertorio, F.; Cremer, P. S., Making Lipid Membranes Rough, Tough, and Ready to Hit the Road. *MRS Bulletin* **2006**, *31*, 536-540.
- 28. Mueller, A.; O'Brien, D. F., Supramolecular Materials Via Polymerization of Mesophases of Hydrated Amphiphiles. *Chemical Reviews* **2002**, *102*, 727-757.
- 29. Cashion, M. P.; Long, T. E., Biomimetic Design and Performance of Polymerizable Lipids. *Acc. Chem. Res.* **2009**, *42*, 1016-1025.
- 30. Fonseka, N. M.; Liang, B. Y.; Orosz, K. S.; Jones, I. W.; Hall, H. K.; Christie, H. S.; Aspinwall, C. A.; Saavedra, S. S., Nanodomain Formation in Planar Supported Lipid

- Bilayers Composed of Fluid and Polymerized Dienoyl Lipids. *Langmuir* **2019**, *35*, 12483-12491.
- 31. Orosz, K. S.; Jones, I. W.; Keogh, J. P.; Smith, C. M.; Griffin, K. R.; Xu, J.; Comi, T. J.; Hall, H. K., Jr.; Saavedra, S. S., Photopolymerization of Dienoyl Lipids Creates Planar Supported Poly(Lipid) Membranes with Retained Fluidity. *Langmuir* **2016**, *32*, 1577-84.
- 32. Okazaki, T.; Inaba, T.; Tatsu, Y.; Tero, R.; Urisu, T.; Morigaki, K., Polymerized Lipid Bilayers on a Solid Substrate: Morphologies and Obstruction of Lateral Diffusion. *Langmuir* **2009**, *25*, 345-351.
- 33. Binder, H.; Dietrich, U.; Schalke, M.; Pfeiffer, H., Hydration-Induced Deformation of Lipid Aggregates Before and After Polymerization. *Langmuir* **1999**, *15*, 4857-4866.
- 34. Evans, E.; Needham, D., Physical Properties of Surfactant Bilayer Membranes: Thermal Transitions, Elasticity, Rigidity, Cohesion, and Colloidal Interactions. *J. Phys. Chem.* **1987**, *91*, 4219-4228.
- 35. Heitz, B. A.; Jones, I. W.; Hall, H. K., Jr.; Aspinwall, C. A.; Saavedra, S. S., Fractional Polymerization of a Suspended Planar Bilayer Creates a Fluid, Highly Stable Membrane for Ion Channel Recordings. *J. Am. Chem. Soc.* **2010**, *132*, 7086-93.
- 36. Nagle, J. F., Experimentally Determined Tilt and Bending Moduli of Single-Component Lipid Bilayers. *Chem. Phys. Lipids.* **2017**, *205*, 18-24.
- 37. Tristram-Nagle, S.; Kim, D. J.; Akhunzada, N.; Kucerka, N.; Mathai, J. C.; Katsaras, J.; Zeidel, M.; Nagle, J. F., Structure and Water Permeability of Fully Hydrated DiphytanoylPC. *Chem. Phys. Lipids* **2010**, *163*, 630-7.
- 38. Kurniawan, J.; Suga, K.; Kuhl, T. L., Interaction Forces and Membrane Charge Tunability: Oleic Acid Containing Membranes in Different pH Conditions. *Biochim. Biophys. Acta Biomembr.* **2017**, *1859*, 211-217.
- 39. Rawicz, W.; Olbrich, K. C.; McIntosh, T.; Needham, D.; Evans, E., Effect of Chain Length and Unsaturation on Elasticity of Lipid Bilayers. *Biophys. J.* **2000**, *79*, 328-339.
- 40. Jones, I. W.; Hall, H. K., Demonstration of a Convergent Approach to Uv-Polymerizable Lipids Bisdenpc and Bissorbpc. *Tetrahedron Lett.* **2011**, *52*, 3699-3701.
- 41. Hutter, J. L.; Bechhoefer, J., Calibration of Atomic-Force Microscope Tips. *Review of Scientific Instruments* **1993**, *64*, 1868-1873.
- 42. Alcaraz, J.; Buscemi, L.; Puig-De-Morales, M.; Colchero, J.; Baró, A.; Navajas, D., Correction of Microrheological Measurements of Soft Samples with Atomic Force Microscopy for the Hydrodynamic Drag on the Cantilever. *Langmuir* **2002**, *18*, 716-721.

- 43. Alessandrini, A.; Facci, P., Nanoscale Mechanical Properties of Lipid Bilayers and Their Relevance in Biomembrane Organization and Function. *Micron* **2012**, *43*, 1212-1223.
- 44. Alessandrini, A.; Seeger, H. M.; Caramaschi, T.; Facci, P., Dynamic Force Spectroscopy on Supported Lipid Bilayers: Effect of Temperature and Sample Preparation. *Biophys. J.* **2012**, *103*, 38-47.
- 45. Alessandrini, A.; Seeger, H. M.; Di Cerbo, A.; Caramaschi, T.; Facci, P., What Do We Really Measure in AFM Punch-through Experiments on Supported Lipid Bilayers? *Soft Matter* **2011**, *7*, 7054.
- 46. Stetter, F. W.; Hugel, T., The Nanomechanical Properties of Lipid Membranes Are Significantly Influenced by the Presence of Ethanol. *Biophys. J.* **2013**, *104*, 1049-55.
- 47. Stetter, F. W. S.; Hyun, S. H.; Brander, S.; Urban, J. M.; Thompson, D. H.; Hugel, T., Nanomechanical Characterization of Lipid Bilayers with AFM-Based Methods. *Polymer* **2016**, *102*, 326-332.
- 48. Zhou, J.; Liang, D.; Contera, S., Effect of Intra-Membrane C60 Fullerenes on the Modulus of Elasticity and the Mechanical Resistance of Gel and Fluid Lipid Bilayers. *Nanoscale* **2015**, *7*, 17102-8.
- 49. Hertz, H., Uber Die Beruhrung Fester Elastischer Korper (on the Contact of Elastic Solids). *J. Reine Angew. Math.* **1881**, *92*, 156 –171.
- 50. Landolt-Bornstein, Numerical Data and Functional Relationships in Science and Technology, Group Iii; Springer: Berlin, 1966; Vol. 1.
- 51. Dimitriadis, E. K.; Horkay, F.; Maresca, J.; Kachar, B.; Chadwick, R. S., Determination of Elastic Moduli of Thin Layers of Soft Material Using the Atomic Force Microscope. *Biophysical Journal* **2002**, *82*, 2798-2810.
- 52. Picas, L.; Rico, F.; Scheuring, S., Direct Measurement of the Mechanical Properties of Lipid Phases in Supported Bilayers. *Biophys. J.* **2012**, *102*, L01-3.
- 53. Arce, F. T.; Meckes, B.; Camp, S. M.; Garcia, J. G. N.; Dudek, S. M.; Lal, R., Heterogeneous Elastic Response of Human Lung Microvascular Endothelial Cells to Barrier Modulating Stimuli. *Nanomed.-Nanotechnol. Biol. Med.* **2013**, *9*, 875-884.
- 54. Terán Arce, P. F. M.; Riera, G. A.; Gorostiza, P.; Sanz, F., Atomic-Layer Expulsion in Nanoindentations on an Ionic Single Crystal. *Appl. Phys. Lett.* **2000**, *77*, 839-841.
- 55. Domke, J.; Radmacher, M., Measuring the Elastic Properties of Thin Polymer Films with the Atomic Force Microscope. *Langmuir* **1998**, *14*, 3320-3325.

- 56. Garcia-Manyes, S.; Oncins, G.; Sanz, F., Effect of Ion-Binding and Chemical Phospholipid Structure on the Nanomechanics of Lipid Bilayers Studied by Force Spectroscopy. *Biophys. J.* **2005**, *89*, 1812-1826.
- 57. Butt, H. J., Measuring Electrostatic, Van Der Waals, and Hydration Forces in Electrolyte Solutions with an Atomic Force Microscope. *Biophysical Journal* **1991**, *60*, 1438-1444.
- 58. Butt, H. J.; Cappella, B.; Kappl, M., Force Measurements with the Atomic Force Microscope: Technique, Interpretation and Applications. *Surface Science Reports* **2005**, *59*, 1-152.
- 59. Sullan, R. M. A.; Shi, W. Q.; Chan, H.; Li, J. K.; Walker, G. C., Mechanical Stability of Phase-Segregated Multicomponent Lipid Bilayers Enhanced by Ps-B-Peo Diblock Copolymers. *Soft Matter* **2013**, *9*, 6245-6253.
- 60. Butt, H. J.; Franz, V., Rupture of Molecular Thin Films Observed in Atomic Force Microscopy. I. Theory. *Phys. Rev. E Stat. Nonlin. Soft Matter Phys.* **2002**, *66*, 031601.
- 61. Li, J. K.; Sullan, R. M.; Zou, S., Atomic Force Microscopy Force Mapping in the Study of Supported Lipid Bilayers. *Langmuir* **2011**, *27*, 1308-13.
- 62. Suarez-Germa, C.; Domenech, O.; Montero, M. T.; Hernandez-Borrell, J., Effect of Lactose Permease Presence on the Structure and Nanomechanics of Two-Component Supported Lipid Bilayers. *Biochim. Biophys. Acta* **2014**, *1838*, 842-852.
- 63. Chiantia, S.; Ries, J.; Kahya, N.; Schwille, P., Combined AFM and Two-Focus SFCS Study of Raft-Exhibiting Model Membranes. *ChemPhysChem* **2006**, *7*, 2409-2418.
- 64. Balleza, D.; Garcia-Arribas, A. B.; Sot, J.; Ruiz-Mirazo, K.; Goni, F. M., Ether-Versus Ester-Linked Phospholipid Bilayers Containing Either Linear or Branched Apolar Chains. *Biophys. J.* **2014**, *107*, 1364-1374.
- 65. Mandić, L.; Sadžak, A.; Strasser, V.; Baranović, G.; Jurašin, D. D.; Sikirić, M. D.; Šegota, S., Enhanced Protection of Biological Membranes During Lipid Peroxidation: Study of the Interactions between Flavonoid Loaded Mesoporous Silica Nanoparticles and Model Cell Membranes. *International Journal of Molecular Sciences* **2019**, *20*.
- 66. Wang, X.; Sanderson, R. N.; Ragan, R., Evaluation of Young's Modulus of Tethered 1-Palmitoyl-2-Oleoyl-Sn-Glycero-3-Phosphocholine Membranes Using Atomic Force Spectroscopy. *J. Phys. Chem. C* **2014**, *118*, 29301-29309.
- 67. Yasmann, A.; Sukharev, S., Properties of Diphytanoyl Phospholipids at the Air-Water Interface. *Langmuir* **2015**, *31*, 350-7.

- 68. Picas, L.; Milhiet, P. E.; Hernández-Borrell, J., Atomic Force Microscopy: A Versatile Tool to Probe the Physical and Chemical Properties of Supported Membranes at the Nanoscale. *Chemistry and Physics of Lipids* **2012**, *165*, 845-860.
- 69. Schillers, H., et al., Standardized Nanomechanical Atomic Force Microscopy Procedure (SNAP) for Measuring Soft and Biological Samples. *Scientific Reports* **2017**, 7.
- 70. Sullan, R. M. A.; Li, J. K.; Zou, S., Quantification of the Nanomechanical Stability of Ceramide-Enriched Domains. *Langmuir* **2009**, *25*, 12874-12877.
- 71. Morigaki, K.; Kiyosue, K.; Taguchi, T., Micropatterned Composite Membranes of Polymerized and Fluid Lipid Bilayers. *Langmuir* **2004**, *20*, 7729-7735.
- 72. Muhandiramlage, T. P.; Cheng, Z.; Roberts, D. L.; Keogh, J. P.; Hall, H. K., Jr.; Aspinwall, C. A., Determination of Pore Sizes and Relative Porosity in Porous Nanoshell Architectures Using Dextran Retention with Single Monomer Resolution and Proton Permeation. *Anal. Chem.* **2012**, *84*, 9754-61.
- 73. Nussio, M. R.; Oncins, G.; Ridelis, I.; Szili, E.; Shapter, J. G.; Sanz, F.; Voelcker, N. H., Nanomechanical Characterization of Phospholipid Bilayer Islands on Flat and Porous Substrates: A Force Spectroscopy Study. *J. Phys. Chem. B* **2009**, *113*, 10339-47.

For Table of Contents Only

